Available online at www.sciencedirect.com
ScienceDirect
Journal of the European Ceramic Society 30 (2010) 2625–2631
www.elsevier.com/locate/jeurceramsoc

Microstructure and properties of ZrB_2–SiC composites prepared by spark plasma sintering using $TaSi_2$ as sintering additive

Chunfeng Hu [a,b], Yoshio Sakka [a,b,c,*], Hidehiko Tanaka [a], Toshiyuki Nishimura [b], Shuqi Guo [d], Salvatore Grasso [b,c]

[a] *World Premier International Research Center (WPI) Initiative on Materials Nanoarchitectonics (MANA), National Institute for Materials Science (NIMS), 1-2-1 Sengen, Tsukuba, Ibaraki 305-0047, Japan*
[b] *Fine Particle Processing Group, Nano Ceramics Center, NIMS, 1-2-1 Sengen, Tsukuba, Ibaraki 305-0047, Japan*
[c] *Graduate School of Pure and Applied Sciences, University of Tsukuba, 1-1-1 Tenodai, Tsukuba, Ibaraki 305-8571, Japan*
[d] *Hybrid Materials Center, NIMS, 1-2-1 Sengen, Tsukuba, Ibaraki 305-0047, Japan*

Received 8 March 2010; received in revised form 4 May 2010; accepted 16 May 2010
Available online 9 June 2010

Abstract

ZrB_2–SiC composites were fabricated by spark plasma sintering (SPS) using $TaSi_2$ as sintering additive. The volume content of SiC was in a range of 10–30% and that of $TaSi_2$ was 10–20% in the initial compositions. The composites could be densified at 1600 °C and the core–shell structure with the core being ZrB_2 and the shell containing both Ta and Zr as $(Zr,Ta)B_2$ appeared in the samples. When the sintering temperature was increased up to 1800 °C, only $(Zr,Ta)B_2$ and SiC phases could be detected in the samples and the core–shell structure disappeared. Generally, the composites with core–shell structure and fine-grained microstructure showed the higher electrical conductivity and Vickers hardness. The completely solid soluted composites with coarse-grained microstructure had the higher thermal conductivity and Young's modulus.

Keywords: Composites; Spark plasma sintering; Microstructure; Properties

1. Introduction

Recently, ZrB_2 has been considered as the promising thermal protective materials for reentry spacecrafts due to its low density (6.11 g/cm^3), high melting point (3250 °C), high elastic modulus (491 GPa), high hardness (23 GPa), high thermal conductivity (56 W/m K), good high temperature oxidation resistance, and excellent thermal shock resistance.[1–4] During the dropping in the atmosphere of earth, the nose cap and leading edge of spacecrafts need to endure the high temperature up to 2200 °C and high speed ions ablation.[5] According to the entry simulation (arc-jet) testing, SiC reinforced ZrB_2 composites possess the remarkable anti-ablation capability and oxidation resistance.[6,7] Also, the introduction of SiC particles into ZrB_2 matrix enhances the fracture toughness of composites from 2 to 4 MPa m$^{1/2}$, which upgrades the use reliability.[8] In previous reports, many works have focused on investigating the *in situ* synthesis, low temperature sintering, particle or whisker toughening, as well as the relationship between microstructure and properties of ZrB_2–SiC composites.[3,9–11] For the investigation branch about low temperature sintering, there are mainly two ways. The first way is using the deoxidized carbides, such as B_4C, WC, or VC, to remove the surface oxides of ZrB_2 for promoting the sintering.[12–14] The second way is selecting the low melting point additives, such as $MoSi_2$ (melting point, 2020 °C) or $TaSi_2$ (melting point, 2040 °C) to form the plastic interface phases.[15–17] For using $TaSi_2$ as sintering aid, Opila et al.[16] and Peng and Speyer[18] found that the introduction of $TaSi_2$ into ZrB_2–SiC could further enhance the oxidation resistance of composites. Additionally, Talmy et al.[19] reported that solid solution appeared in ZrB_2–10, 20, and 30 vol.% $TaSi_2$ composites sintered at 2000 °C by hot pressing, which formed the core–shell structure with the core being ZrB_2 and the shell containing both Ta and Zr as $(Zr,Ta)B_2$. This phenomenon was associated with the decomposition of

* Corresponding author at: Nano Ceramics Center, National Institute for Materials Science (NIMS), 1-2-1 Sengen, Tsukuba, Ibaraki 305-0047, Japan. Tel.: +81 29 859 2461; fax: +81 29 859 2401.
E-mail address: SAKKA.Yoshio@nims.go.jp (Y. Sakka).

0955-2219/$ – see front matter © 2010 Elsevier Ltd. All rights reserved.
doi:10.1016/j.jeurceramsoc.2010.05.013

Table 1
Initial compositions for preparing ZrB_2–SiC composites.

Compositions	1010	2010	3010	2020	3020
ZrB_2 (vol.%)	80	70	60	60	50
SiC (vol.%)	10	20	30	20	30
$TaSi_2$ (vol.%)	10	10	10	20	20

$TaSi_2$ and solid solution between Ta–Si phase and ZrB_2, which was proved by Sciti et al.[20] who found that Ta_xSi_y phase containing a certain amount of Zr existed in ZrB_2–15 vol.% $TaSi_2$ composite prepared by hot pressing at 1850 °C. The core–shell structure indicates the heterogeneous microstructure characteristic of composites. It is a sub-stable structure which is prone to become stable by atoms diffusion. For eliminating the core–shell structure of crystals, Talmy et al.[19] considered that an increase in holding time probably contributed to complete the formation of the solid solutions.

In present work, dense bulk ZrB_2–SiC composites were fabricated at 1600–1800 °C by spark plasma sintering using $TaSi_2$ as additive.[21–23] It was found that increasing the sintering temperature was an effective way to remove the core–shell structure. The microstructure, physical, and mechanical properties of as-prepared ZrB_2–SiC composites with and without core–shell structure were investigated and compared.

2. Experimental procedures

Commercial ZrB_2 (99%, 2 μm) (Rare Metallic Co., Ltd., Japan), α-SiC (99%, 0.55 μm) (Yakushima Denko Co., Ltd., Japan), and $TaSi_2$ (99%, 2–5 μm) (Japan New Metals Co., Ltd., Japan) powders were used to fabricate the composites. The designed initial compositions are listed in Table 1. The volume content of SiC was in a range of 10–30%, and that of $TaSi_2$ was 10–20%. The powders were weighed by an electrical balance with the accuracy of 10^{-2} g. The weighed powders were mixed for 24 h in a SiC jar with ethanol as the dispersant. The milling media were silicon carbide balls. After milling, the mixtures were dried in air and then sieved using a 125 mesh sieve. Firstly, the mixture was put into a graphite die with a diameter of 20 mm. A layer of flexile graphite paper (∼0.2 mm thickness) was put into the inner part of die for lubrication, and a layer of carbon fiber was used to wrap the die for inhibiting the rapid heat diffusion. Then the mixture was cold-pressed as a compact green and the green together with the die was heated in a spark plasma sintering facility (100 kN SPS-1050, Syntex Inc., Japan) in vacuum (10^{-2} Pa). Each pulse lasted 3.3 ms and the duty cycle was 12 pulses on and 2 pulses off. The sintering temperature was measured by an optical pyrometer focusing on a hole in the wall of die. From ambient temperature to 700 °C, it took 5 min to heat the sample. Then the temperature was increased up to annealing temperature with a heating rate of 100 °C/min. The annealing temperatures were selected as 1600 and 1800 °C, respectively. The vacuum level was recorded in turn of residual pressure. The holding time was 5 min. The sintering displacement versus temperature was recorded simultaneously and at last corrected using a known thermal expansion of graphite die. During the sintering, the uniaxial pressure was increased up to 30 MPa before 1000 °C. After sintering, the sample was cooled down to ambient temperature with the cooling rate of furnace. The contaminations on the surface of samples were removed by a diamond grinding wheel. Respectively, the sintered samples were denoted as ZS*n* (*n* = 1–10) (Table 2).

All the samples were ground and polished down to 1.0 μm diamond grits. The densities of as-prepared samples were measured by the Archimedes method. Phase compositions in the samples were examined by an X-ray diffraction (XRD) analyzer (JDX-3500, JEOL Ltd., Japan) with Cu Kα radiation. The scanning speed was 2°/min. Lattice parameters of solid soluted hexagonal ZrB_2 were calculated according to the interplaner spacing equation and Bragg equation based on the XRD data. The morphologies of polished and fracture surface of samples were investigated by a scanning electron microscope (SEM) (JSM-6500, JEOL Ltd., Japan) equipped with an energy dispersive spectroscopy (EDS) system. Vickers hardness measurement was conducted by a microhardness tester (MVK-E, Akashi Co., Japan) under a load of 9.8 N. For each sample, nine indents were made. The elastic property was evaluated by an ultrasonic equipment (TDS 3034B, Tektronix Inc., USA). For each sample, it was tested for three times. The evaluation of fracture toughness of samples was conducted by an indentation microfracture (IM) method. A hardness tester (AVK-A, Akashi Co., Japan) was adopted to produce the diagonal cracks. The applied load was 49 N. The lengths of diagonal cracks were

Table 2
Typical physical and mechanical properties of ZrB_2–SiC composites sintered at 1600 °C (ZS1–5) and 1800 °C (ZS6–10) by spark plasma sintering.

Samples	Sintering temperature (°C)	Density (g/cm^3)	Electrical conductivity ($\times 10^5\ \Omega^{-1}\ m^{-1}$)	Thermal conductivity (W/m K)	Vickers hardness (GPa)	Fracture toughness (MPa m$^{1/2}$)	Young's modulus (GPa)
ZS1(1010)	1600	5.50	16.18 ± 1.42	42.89 ± 0.50	19.8 ± 0.8	4.03 ± 0.28	453.7 ± 0.8
ZS2(2010)	1600	5.30	12.83 ± 1.78	45.25 ± 0.51	20.7 ± 0.9	4.02 ± 0.74	459.3 ± 1.7
ZS3(3010)	1600	5.07	8.07 ± 0.63	44.90 ± 0.49	22.4 ± 1.6	4.47 ± 0.36	453.6 ± 1.4
ZS4(2020)	1600	5.59	10.19 ± 1.19	39.82 ± 0.29	21.8 ± 0.8	4.58 ± 0.18	450.7 ± 1.6
ZS5(3020)	1600	5.32	5.82 ± 1.05	46.32 ± 0.17	21.5 ± 1.7	4.79 ± 0.44	437.6 ± 1.5
ZS6(1010)	1800	5.50	14.46 ± 0.96	45.60 ± 0.48	20.8 ± 1.3	4.03 ± 0.61	463.9 ± 1.6
ZS7(2010)	1800	5.34	13.66 ± 0.79	46.92 ± 0.15	19.4 ± 1.3	4.40 ± 0.96	463.2 ± 1.0
ZS8(3010)	1800	5.11	8.25 ± 0.40	53.33 ± 0.47	21.2 ± 1.2	4.59 ± 0.61	460.7 ± 0.7
ZS9(2020)	1800	5.64	8.89 ± 0.61	46.99 ± 0.78	20.3 ± 0.7	4.89 ± 0.78	453.1 ± 1.3
ZS10(3020)	1800	5.42	5.20 ± 0.25	51.35 ± 0.52	20.1 ± 0.8	4.76 ± 0.41	452.9 ± 0.6

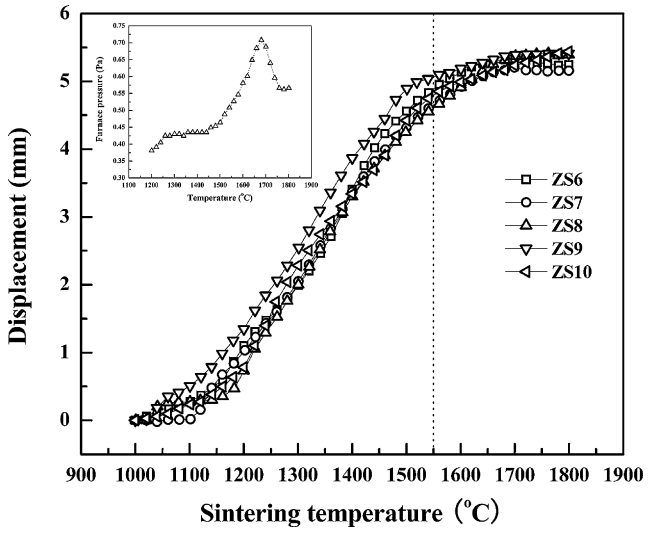

Fig. 1. Displacement as a function of sintering temperature during spark plasma sintering. Inner figure shows the furnace pressure change for ZS8 sample.

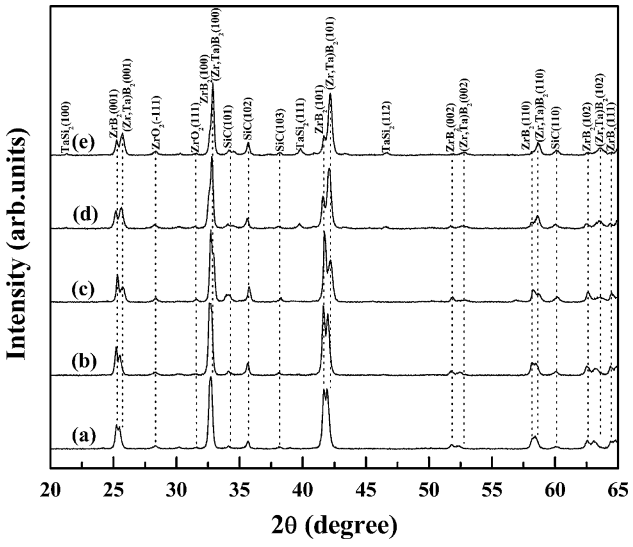

Fig. 2. X-ray diffraction (XRD) patterns of ZrB_2–SiC composites with $TaSi_2$ additive sintered at 1600 °C: (a) ZS1, (b) ZS2, (c) ZS3, (d) ZS4, and (e) ZS5.

measured by SEM. For each sample, six indents were used. The electrical conductivity was measured using the four-wire probe at room temperature. The applied constant current was 50 mA supplied by a DC precision current source (Model 6220, Keithley, OH). The current–voltage (*IV*) characteristics of samples were recorded using a digital nanovoltmeter (Model 2182, Keithley, OH). Additionally, thermal conductivity measurement was performed by a Xenon flash apparatus (LFA447 Nanoflash, NETZSCH, Germany) at room temperature. A disk specimen with a dimension of Φ10 mm × 2 mm was used. A layer of colloidal graphite spray was coated on the surface of sample for enhancing the absorption of Xenon light pulse energy and the emission of infrared (IR) radiation to the temperature detector.

3. Results and discussion

3.1. Synthesis and microstructure

Fig. 1 shows the sintering displacement curves versus sintering temperature up to 1800 °C. It is seen that above 1550 °C the slope of sintering displacement begins to decrease. When the sintering temperature is above 1680 °C, the displacement approaches a constant. Additionally, it is observed that when the sintering temperature is above 1500 °C the furnace pressure increases rapidly; while above 1680 °C, the furnace pressure decreases rapidly. From 1100 to 1550 °C, the large slope of displacement might be ascribed to the rapid decrease of porosity in the sintered samples. In present composites, $TaSi_2$ was added for improving the sinterability. It is known that the melting point of $TaSi_2$ is 2040 and 1550 °C is close to the 0.8 of melting point (1632 °C).[24] The plastic deformation of $TaSi_2$ at high temperature might induce the continuous increase of displacement above 1550 °C. However, the plastic deformation was comparatively slow corresponding to the decrement of displacement slope. In addition, the solid solution of Ta atoms into ZrB_2 could form $(Zr,Ta)B_2$.[19] The decomposed silicon from $TaSi_2$ probably evaporated in the high vacuum, which was associated with the increase of furnace pressure. Above 1680 °C, the solid solution of Ta atoms into ZrB_2 might have completed and the silicon was still evaporating from the samples but the total amount of silicon in sample was decreasing. Therefore, the furnace pressure declined. At 1800 °C, the furnace pressure reached stability, which might be ascribed to the complete evaporation of silicon. It is considered that when the composites were sintered at 1600 °C, the solid solution was formed and the core–shell structure probably existed in the composites. And when the sintering temperature was increased up to 1800 °C, the solid solution was completed and the core–shell structure possibly disappeared. Therefore, 1600 and 1800 °C were selected for preparing the composites with and without core–shell structure.

Fig. 2 displays the X-ray diffraction patterns of composites sintered at 1600 °C. It is obviously seen that in the composites the solid solution $(Zr,Ta)B_2$ coexists with ZrB_2. In ZS1–3 samples, ZrB_2 is the main phase; while in ZS4 and ZS5, $(Zr,Ta)B_2$ becomes the primary component. In ZS1–3, $TaSi_2$ has completely disappeared; and in ZS4 and ZS5, just few $TaSi_2$ exist due to the incomplete decomposition. That is, the final content of SiC in the ZS1–5 composites has changed, as about 11.11, 22.22, 33.33, 25, and 37.5 vol.%, respectively. With more SiC and $TaSi_2$, i.e., the less ZrB_2 in the initial compositions, the diffraction peaks of $(Zr,Ta)B_2$ in the sintered samples deflect to higher angles. It is known that Ta atom radius (0.146 nm) is smaller than that of Zr (0.162 nm).[25,26] The introduction of Ta atoms into ZrB_2 would constrict its crystal structure, leading to the decrease of lattice parameters.[19] The calculated *c* value of $(Zr,Ta)B_2$ gradually decreases as 0.3501, 0.3490, 0.3484, 0.3472, and 0.3469 nm in ZS1–5 samples, which means that the Ta molar ratio in $(Zr,Ta)B_2$ gradually increases in the order of ZS1–5. Additionally, a little ZrO_2 were detected in the composites, which might be introduced during the milling process.[27] When the sintering temperature was increased up to 1800 °C, the XRD spectra of composites are shown in Fig. 3. Obviously, it is seen that no diffraction peaks of ZrB_2 exist again. The diffraction

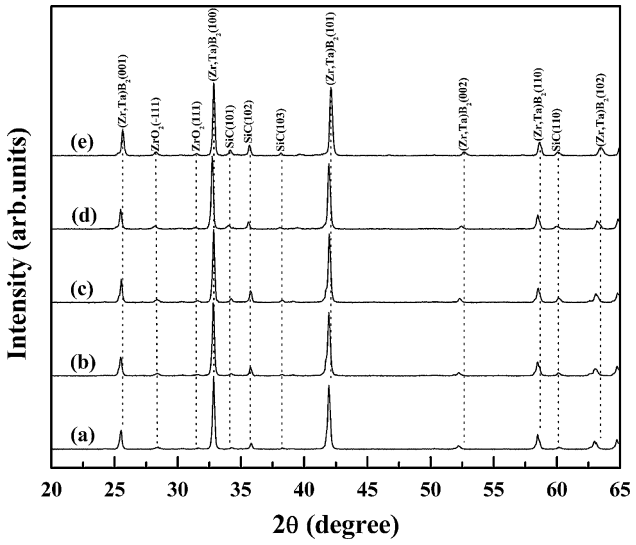

Fig. 3. XRD patterns of ZrB_2–SiC composites with $TaSi_2$ additive sintered at 1800 °C: (a) ZS6, (b) ZS7, (c) ZS8, (d) ZS9, and (e) ZS10.

peaks of (Zr,Ta)B_2 deflect to the higher angles in the order of ZS6–10. The calculated *c* value of (Zr,Ta)B_2 also shows the gradual decrease as 0.3511, 0.3501, 0.3498, 0.3485, and 0.3481 nm in ZS6–10 specimens, which indicates the gradual increase of Ta molar ratio in (Zr,Ta)B_2 solid solution. In addition, by comparing the *c* values of (Zr,Ta)B_2 in the samples sintered at 1600 and 1800 °C using the same initial compositions, it is seen that those in the composites synthesized at 1600 °C are higher. It is revealed that when the samples were sintered at 1600 °C, the shell structure probably caused the separation of diffraction peaks due to the solid solution. The shell possessed the higher Ta molar ratio in comparison with core. While when the samples were fabricated at 1800 °C, solid solution completed in the composites, i.e., Ta atoms have homogeneously distributed in the (Zr,Ta)B_2 grains, and the core–shell structure has disappeared corresponding to the disappearance of ZrB_2 diffraction peaks. Therefore, Ta molar ratios of (Zr,Ta)B_2 in the samples sintered at 1800 °C are lower than those of corresponding specimens prepared at 1600 °C under the same initial compositions.

Fig. 4 shows the polished surface of ZS1 and ZS6 sintered at 1600 and 1800 °C, respectively. It is observed that the core–shell structure apparently exists in the ZS1 sample fabricated at 1600 °C (Fig. 4(a)). (Zr,Ta)B_2 solid solution (grey-white) distributes around ZrB_2 grains (grey-black) to form shell. At 1800 °C, the (Zr,Ta)B_2 solid solution homogeneously distributes in the ZS6 sample and no single phase ZrB_2 could be detected by EDS analysis (Fig. 4(b)). The insert EDS pattern shows that the grey-white grains combine the elements of Zr, Ta, and B as (Zr,Ta)B_2. Fig. 5 shows the polished and fracture surface of ZS4 and ZS9 samples. No apparent pores can be observed in the polished surface of samples, which indicates the full densification of composites. In Fig. 5(a), the polished surface shows the typical core–shell grains combining the SiC particles; while in Fig. 5(c), only single phase (Zr,Ta)B_2 and SiC can be found. In the fracture surface of ZS4 sample, the dominant fracture mode is transgranular (Fig. 5(b)), which is probably

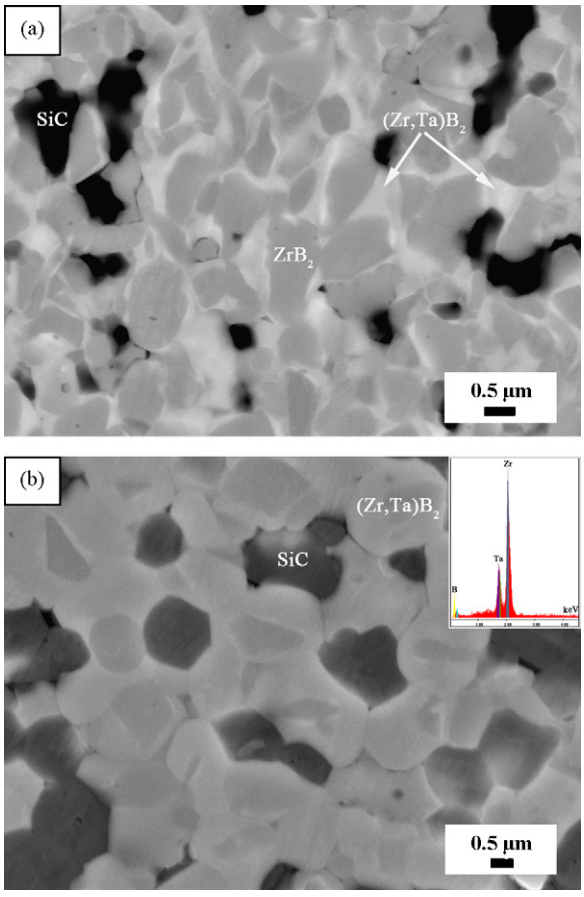

Fig. 4. Scanning electron microscope (SEM) micrographs of polished surface of (a) ZS1 and (b) ZS6, showing the phase distribution of ZrB_2 (grey-black), (Zr,Ta)B_2 (grey-white), and SiC (black). Insert in (b) is the energy dispersive spectroscopy (EDS) analysis of (Zr,Ta)B_2 grain.

ascribed to the strong bonding among (Zr,Ta)B_2 shells. In the fracture surface of ZS9, there are the multiplex fracture modes including transgranular and intergranular (Fig. 5(d)). The bigger particle size of (Zr,Ta)B_2 and SiC in ZS9 sample might be attributed to the growth of particles when sintered at higher temperature. The mean grain sizes of core–shell ZrB_2 and SiC in ZS4 are close to the initial powders as 2 and 0.55 μm, respectively. It means that at low temperature the sintering did not accelerate the growth of particles. However, the average particle sizes of solid solution (Zr,Ta)B_2 and SiC in ZS9 are 4 and 2 μm, respectively. That is, the composites sintered at 1600 °C possess the finer microstructure.

3.2. Physical and mechanical properties

The typical physical and mechanical properties of composites are listed in Table 2. It is seen that the electrical conductivity of composites with the same volume content of $TaSi_2$ additive decreases with increasing SiC volume content when sintered at the same temperature. When the samples were prepared at 1600 °C, the electrical conductivity of composites (ZS1–3) containing 10 vol.% $TaSi_2$ in the initial compositions decreases from 16.18 to $8.07 \times 10^5\ \Omega^{-1}\ m^{-1}$ and those of samples (ZS4 and 5) containing 20 vol.% $TaSi_2$ in the initial compositions decreases

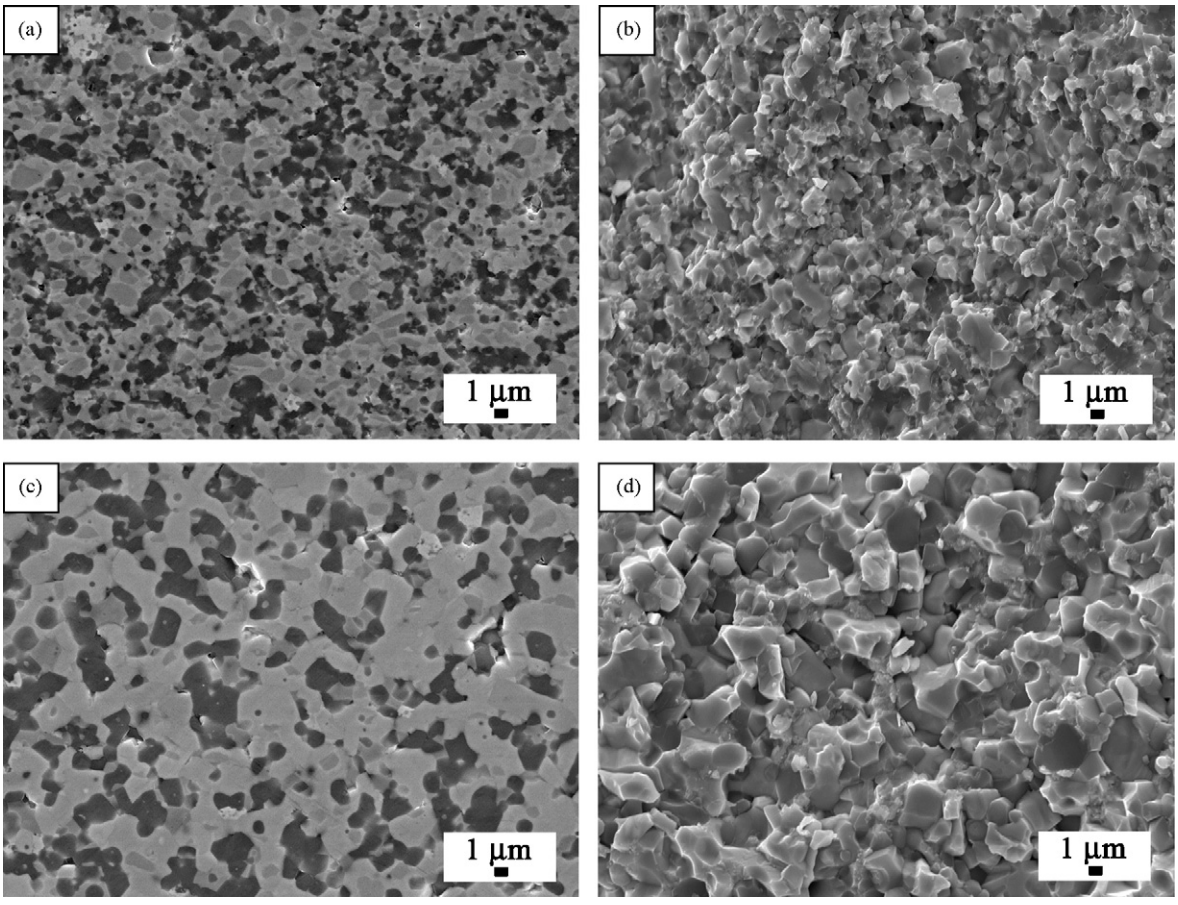

Fig. 5. SEM micrographs of polished and fracture surface of (a) and (b) ZS4, and (c) and (d) ZS9.

from 10.19 to $5.82 \times 10^5\ \Omega^{-1}\ m^{-1}$. For the samples sintered at 1800 °C, the electrical conductivity of composites also yields the same decreasing tendency with increasing SiC content. The electrical conductivity of ZS6–8 composites decreases from 14.46 to $8.25 \times 10^5\ \Omega^{-1}\ m^{-1}$, and those of ZS9 and ZS10 specimens declines from 8.89 to $5.20 \times 10^5\ \Omega^{-1}\ m^{-1}$. This decrease is mainly due to the increasing content of low electrical conductive SiC (semiconductor).[8] Probably, there is another reason that the formation of (Zr,Ta)B_2 solid solution would decrease the electrical conductivity because of the lower electrical conductivity of TaB_2 (about $1.16 \times 10^6\ \Omega^{-1}\ m^{-1}$) than that of ZrB_2 (about $4.55 \times 10^6\ \Omega^{-1}\ m^{-1}$).[28] Similarly, Rahman et al.[29] has determined that in the ZrB_2–TiB_2 system the solid solution of Ti atoms into ZrB_2 decreased the electrical conductivity due to the higher room temperature resistivity of TiB_2. It is considered that more Ta atoms entering into ZrB_2, i.e., higher Ta molar ratio, would lead to lower electrical conductivity of (Zr,Ta)B_2. In addition, by comparing the composites prepared using the same volume content of SiC in the initial compositions and sintered at the same temperature, it is seen that the electrical conductivity decreases with the increment of $TaSi_2$. In comparison with ZS4 and ZS5, ZS2 and ZS3 show the higher electrical conductivity, respectively. Possibly, it is due to the less volume content of ZrB_2 and (Zr,Ta)B_2 and the higher Ta molar ratios of (Zr,Ta)B_2 in ZS4 and ZS5. Also, ZS7 and ZS8 show the higher values of electrical conductivity in comparison with ZS9 and ZS10, respectively, which is probably associated with the less (Zr,Ta)B_2 content and higher Ta molar ratios of (Zr,Ta)B_2 in ZS9 and ZS10. On the other hand, it is known that the core–shell structure exists in ZS1–5 but disappears in ZS6–10. By comparing the electrical conductivity of ZS6–10 with those of ZS1–5 one by one, it is seen that except ZS7 and ZS8 the samples of ZS6, ZS9, and ZS10 show the lower electrical conductivity. In ZS1, ZS4, and ZS5, it has been known that the solid soluted (Zr,Ta)B_2 has the higher Ta molar ratio, indicating the lower electrical conductivity of (Zr,Ta)B_2. However, the main phase is ZrB_2 in ZS1. In previous investigations, it has also been found that the increase of grain size in materials decreases the electrical conductivity.[30–32] Probably, it can be explained why ZS1 has the higher electrical conductivity than that of ZS6. Similarly, though (Zr,Ta)B_2 solid solution is the main component in ZS4 and ZS5, the fine-grained microstructure might be the dominant factor for the higher electrical conductivity. That is, the competition might exist between solid solution and microstructure, which probably also induces the abnormal increase of electrical conductivity in ZS7 and ZS8.

Additionally, for investigating the thermal conductivity of composites, it is observed that with the increasing SiC content the thermal conductivity of specimens generally increases under the same volume content of $TaSi_2$ additive when prepared at the same temperature. Zimmermann et al.[28] has proved that at room temperature ZrB_2–30 vol.% SiC composite pos-

sessed the higher thermal conductivity (62 W/m K) than single phase ZrB_2 (53 W/m K). Guo et al.[33] also confirmed that in ZrC–ZrB_2–SiC composites the thermal conductivity increased with the higher molar content of SiC due to the reason that SiC had the higher thermal conductivity than ZrB_2. For the samples fabricated at 1600 °C (ZS1–5), except ZS3 sample, the increase tendency of thermal conductivity is clear. ZS5 specimen has the highest thermal conductivity of 46.32 W/m K based on the highest SiC content. For these samples sintered at 1800 °C (ZS6–10), the thermal conductivity of ZS6–8 increase from 45.60 to 53.33 W/m K, and those of ZS9 and ZS10 are 46.99 and 51.35 W/m K, respectively. Whereas, for the composites containing same SiC content in the initial compositions and sintered at the same temperature, the thermal conductivity does not obey one rule of increase or decrease with the increment of $TaSi_2$ additive. It is known that the thermal conductivity of composites is associated with the phase compositions and interfacial thermal resistivity between phases.[8] Probably, the competitive relationship exists between them. Furthermore, by comparing the samples prepared at 1600 and 1800 °C using the same initial compositions, it is obviously seen that the samples sintered at 1800 °C show the higher thermal conductivity. It has been proved that the formation of solid solution decreases the thermal conductivity of ceramics due to the degradation of phonon mean free path caused by the mass disorder on the cation sublattice.[34] The higher Ta molar ratio would lead to the lower thermal conductivity of (Zr,Ta)B_2 solid solution in present composites.[35] It means that the corresponding (Zr,Ta)B_2 in ZS1–5 has the lower thermal conductivity than that in ZS6–10 due to the higher Ta molar ratio. Also, for dense ceramics, the larger mean grain size yields a significant increase about ambient thermal conductivity due to a reduction of the number of grain boundaries in the heat flow path.[36] Possibly, it can be understood why ZS6–10 have the higher thermal conductivity.

Also, the Vickers hardness, fracture toughness, and Young's moduli of composites were investigated and compared. About the Vickers hardness, it is found that for ZS1–5 samples sintered at 1600 °C the hardness values are in a range of 19.8–22.4 GPa and those of ZS6–10 prepared at 1800 °C are 19.4–21.2 GPa. There is no obvious hardness change tendency with the increasing SiC or $TaSi_2$ content in the initial compositions when sintered at the same temperature. It means that the hardness of present composites is not sensitive to component difference when prepared at the same temperature. Additionally, through comparing the samples sintered at 1600 and 1800 °C using the same initial compositions one by one, it is found that except ZS1 the Vickers hardness of specimens sintered at 1600 °C are higher than those of samples prepared at 1800 °C, which is possibly attributed to the finer microstructure.[37] It has been proved that the fine-grained ceramic possesses the higher scratch hardness and Vickers hardness under the same testing condition in comparison with the coarse-grained sample.[38] Additionally, considering another factor of solid solution, it has been determined that ZrB_2 (23 GPa) shows the higher hardness than TaB_2 (21 GPa).[39] Probably, the solid solution of Ta atoms into ZrB_2 would decrease the hardness by forming (Zr,Ta)B_2 solid solution, and the higher Ta molar ratio in (Zr,Ta)B_2 indicates the lower Vickers hardness. The competitive effect on the hardness might exist between fine microstructure and solid solution. Obviously, the higher hardness of samples sintered at 1600 °C are mainly determined by the fine microstructure.

For the fracture toughness of as-prepared samples, they are nearly at the same degree of 4 MPa $m^{1/2}$. It is considered that the fracture toughness is almost independent with the component and microstructure of present composites prepared at 1600 and 1800 °C. In addition, the Young's moduli of all composites sintered at 1600 and 1800 °C exhibit the high values of 437.6–463.9 GPa. Generally, the Young's moduli of composites show the decrease tendency with increasing SiC volume content under the same $TaSi_2$ additive when prepared at the same temperature, which might be ascribed to the low elastic modulus of SiC (415 GPa) in comparison with ZrB_2 (491 GPa) based on the mixture rule.[40,41] Additionally, by comparing the composites sintered using the same SiC content but different $TaSi_2$ contents in the initial compositions, it is observed that the Young's moduli of composites prepared at the same temperature decrease with the increment of $TaSi_2$. For the samples sintered at 1600 °C, ZS2 and ZS3 have the higher modulus values of 459.3 and 453.6 GPa when compared with those of ZS4 (450.7 GPa) and ZS5 (437.6 GPa), respectively. For these composites prepared at 1800 °C, the Young's moduli of ZS7 and ZS8 are 463.2 and 460.7 GPa, respectively, higher than those of corresponding ZS9 (453.1 GPa) and ZS10 (452.9 GPa). The reason is also possibly attributed to the final more SiC content in ZS4, ZS5, ZS9 and ZS10 due to the decomposition of $TaSi_2$ and solid solution of Ta atoms into ZrB_2. On the other hand, when the Young's moduli of composites sintered at 1600 and 1800 °C are compared, it is seen that the modulus values of samples sintered at 1800 °C are higher than those of specimens prepared at 1600 °C using the same initial compositions. Because the true densities of dense samples sintered at 1600 and 1800 °C using the same initial compositions are close, it is considered that the effect of pores on Young's modulus can be ignored. Also, the particle sizes in the composites are not different so much (Fig. 5) and just in the scale of micrometer, which should not impose the evident effect on the Young's modulus.[42,43] Therefore, the only reason is associated with the solid solution. It is known that the Young's modulus of TaB_2 is 551 GPa, higher than that of ZrB_2 (491 GPa).[44] It is believed that the introduction of Ta atoms into ZrB_2 would enhance the Young's modulus by forming (Zr,Ta)B_2 solid solution. The Ta molar ratios in the shell of ZS1–5 samples are higher than those of (Zr,Ta)B_2 in ZS6–10, respectively, which indicates the higher Young's modulus. However, due to the existence of ZrB_2 in ZS1–5, the average Young's moduli of ZS1–5 are lower than those of ZS6–10, respectively.

4. Conclusions

ZrB_2–SiC composites were synthesized by SPS using $TaSi_2$ as the sintering additive. The volume content of SiC was in the range of 10–30% and that of $TaSi_2$ was 10–20% in the initial compositions. It was found that when the composites were densified at 1600 °C, the core–shell structure with the core being ZrB_2 and the shell containing both Ta and Zr as (Zr,Ta)B_2 appeared in

the composites. When the sintering temperature was increased up to 1800 °C, the core–shell structure disappeared and only (Zr,Ta)B_2 and SiC phases existed in the composites. Generally, the composites with core–shell and fine-grained microstructure showed the higher electrical conductivity and Vickers hardness. The completely solid soluted composites with coarse-grained microstructure had the higher thermal conductivity and Young's modulus.

Acknowledgements

This work was partially supported by Grand-in-Aid for Scientific Research from the JSPS of Japan and also World Premier International Research Center (WPI) Initiative, MEXT, Japan.

References

1. Mroz C. Zirconium diboride. *Am Ceram Soc Bull* 1994;**73**:141–2.
2. Telle R, Sigl LS, Takagi K. In: Riedel R, editor. *Boride-based hard materials. Hand-book of ceramic hard materials*. Weinheim, Germany: Wiley–VCH; 2000. p. 803–945.
3. Chamberlain AL, Fahrenholtz WG, Hilmas GE, Ellerby DT. High strength zirconium diboride-based ceramics. *J Am Ceram Soc* 2004;**87**:1170–2.
4. Ni DW, Zhang GJ, Kan YM, Sakka Y. Highly textured ZrB_2-based ultrahigh temperature ceramics via strong magnetic field alignment. *Scripta Mater* 2009;**60**:615–8.
5. Borrelli R, Riccio A, Tescione D, Gardi R, Marino G. Thermo-structural behaviour of an UHTC made nose cap of a reentry vehicle. *Acta Astronaut* 2009;**65**:442–56.
6. Monteverde F, Savino R. Stability of ultra-high-temperature ZrB_2–SiC ceramics under simulated atmospheric re-entry conditions. *J Eur Ceram Soc* 2007;**27**:4797–805.
7. Bull J, White MJ, Kaufman L. Ablation resistant zirconium and hafnium ceramics. *United States Patent 5,750,450*; 12 May 1998.
8. Guo SQ. Densification of ZrB_2-based composites and their mechanical and physical properties: a review. *J Eur Ceram Soc* 2009;**29**:995–1011.
9. Zhang GJ, Deng ZY, Kondo N, Yang JF, Ohji T. Reactive hot pressing of ZrB_2–SiC composites. *J Am Ceram Soc* 2000;**83**:2330–2.
10. Guo SQ, Nishimura T, Mizuguchi T, Kagawa Y. Mechanical properties of hot-pressed ZrB_2–$MoSi_2$–SiC composites. *J Eur Ceram Soc* 2008;**28**:1891–8.
11. Zhang XH, Xu L, Du SY, Liu CY, Han JC, Han WB. Spark plasma sintering and hot pressing of ZrB_2–SiCw ultra-high temperature ceramics. *J Alloys Compd* 2008;**466**:241–5.
12. Zhang H, Yan YJ, Huang ZR, Liu XJ, Jiang DL. Pressureless sintering of ZrB_2–SiC ceramics: the effect of B_4C content. *Scripta Mater* 2009;**60**:559–62.
13. Zou J, Zhang GJ, Kan YM. Formation of tough interlocking microstructure in ZrB_2–SiC-based ultrahigh-temperature ceramics by pressureless sintering. *J Mater Res* 2009;**24**:2428–34.
14. Zou J, Zhang GJ, Kan YM, Wang PL. Pressureless densification of ZrB_2–SiC composites with vanadium carbide. *Scripta Mater* 2008;**59**:309–12.
15. Guo SQ, Kagawa Y, Nishimura T, Tanaka H. Thermal and electric properties in hot-pressed ZrB_2–$MoSi_2$–SiC composites. *J Am Ceram Soc* 2007;**90**:2255–8.
16. Opila E, Levine S, Lorincz J. Oxidation of ZrB_2- and HfB_2-based ultra-high temperature ceramics: effect of Ta additions. *J Mater Sci* 2004;**39**:5969–77.
17. Peng F, Berta Y, Speyer RF. Effect of SiC, TaB_2 and $TaSi_2$ additives on the isothermal oxidation resistance of fully dense zirconium diboride. *J Mater Res* 2009;**24**:1855–67.
18. Peng F, Speyer RF. Oxidation resistance of fully dense ZrB_2 with SiC, TaB_2, and $TaSi_2$ additives. *J Am Ceram Soc* 2008;**91**:1489–94.
19. Talmy IG, Zaykoski JA, Opeka MM. High-temperature chemistry and oxidation of ZrB_2 ceramics containing SiC, Si_3N_4, Ta_5Si_3, and $TaSi_2$. *J Am Ceram Soc* 2008;**91**:2250–7.
20. Sciti D, Silvestroni L, Celotti G, Melandri C, Guicciardi S. Sintering and mechanical properties of ZrB_2–$TaSi_2$ and HfB_2–$TaSi_2$ ceramic composites. *J Am Ceram Soc* 2008;**91**:3285–91.
21. Maizza G, Grasso S, Sakka Y, Noda T, Ohashi S. Relation between microstructure, properties and spark plasma sintering (SPS) parameters of pure ultrafine WC powder. *Sci Technol Adv Mater* 2007;**8**:644–54.
22. Orrù R, Licheri R, Locci AM, Cincotti A, Cao G. Consolidation/synthesis of materials by electric current activated/assisted sintering. *Mater Sci Eng R* 2009;**63**:127–287.
23. Grasso S, Sakka Y, Maizza G. Electric current activated/assisted sintering (ECAS): a review of patents 1906–2008. *Sci Technol Adv Mater* 2009;**10**:053001.
24. Hu CF, He LF, Li FZ, Wu L, Wang JY, Li MS, Bao YW, Zhou YC. *In situ* reaction synthesis and mechanical properties of TaC–$TaSi_2$ composites. *Int J Appl Ceram Technol*; in press.
25. Pérez RA, Dyment F, Bermúdez GG, Abriola D, Behar M. Diffusion of Ta in α-Ti. *Appl Phys A* 2003;**76**:247–50.
26. Saida J, Sanada T, Sato S, Imafuku M, Li CF, Inoue A. Nano quasicrystal formation and local atomic structure in Zr–Pd and Zr–Pt binary metallic glasses. *Z Kristallogr* 2008;**223**:726–30.
27. Lee SH, Sakka Y, Kagawa Y. Dispersion behavior of ZrB_2 powder in aqueous solution. *J Am Ceram Soc* 2007;**90**:3455–9.
28. Zimmermann JW, Hilmas GE, Fahrenholtz WG, Dinwiddie RB, Porter WD, Wang H. Thermophysical properties of ZrB_2 and ZrB_2–SiC ceramics. *J Am Ceram Soc* 2008;**91**:1405–11.
29. Rahman M, Wang CC, Chen WH, Akbar SA, Mroz C. Electrical resistivity of titanium diboride and zirconium diboride. *J Am Ceram Soc* 1995;**78**:1380–2.
30. Tschöpe A, Birringer R. Grain size dependence of electrical conductivity in polycrystalline cerium oxide. *J Electroceram* 2001;**7**:169–77.
31. Joshi DP, Sen K. Effect of grain size on the resistiviy of polycrystalline material. *Solar Cells* 1983;**9**:261–7.
32. Li J, Lü XJ, Li QY, Lai YQ, Yang JH. Electrical resistivity of TiB_2/C composite cathode coating for aluminum electrolysis. *J Cent South Univ Technol* 2006;**13**:209–13.
33. Guo SQ, Kagawa Y, Nishimura T, Chung DH, Yang JM. Mechanical and physical behavior of spark plasma sintered ZrC–ZrB_2–SiC composites. *J Eur Ceram Soc* 2008;**28**:1279–85.
34. Winter MR, Clarke DR. Thermal conductivity of yttria-stabilized zirconia–hafnia solid solutions. *Acta Mater* 2006;**54**:5051–9.
35. Wu J, Padture NP, Klemens PG, Gell M, García E, Miranzo P, et al. Thermal conductivity of ceramics in the ZrO_2–$GdO_{1.5}$ system. *J Mater Res* 2002;**17**:3193–200.
36. Fayette S, Smith DS, Smith A, Martin C. Influence of grain size on the thermal conductivity of tin oxide ceramics. *J Eur Ceram Soc* 2000;**20**:297–302.
37. Hu CF, He LF, Liu MY, Wang XH, Wang JY, Li MS, et al. *In situ* reaction synthesis and mechanical properties of V_2AlC. *J Am Ceram Soc* 2008;**91**:4029–35.
38. Xu HHK, Jahanmir S. Effect of grain size on scratch damage and hardness of alumina. *J Mater Sci Lett* 1995;**14**:736–9.
39. Holleck H. Material selection for hard coatings. *J Vac Sci Technol A* 1986;**4**:2661–9.
40. Munro RG. Material properties of a sintered α-SiC. *J Phys Chem Ref Data* 1997;**26**:1195–203.
41. Reuss A. Berechnung der fliessgrenz von mischkristallen auf grund der plastizitätsbedingung für einkristalle. *Z Angew Math Mech* 1929;**9**:49–58.
42. Bréchignac C, Houdy P, Lahmani M. *Nanomaterials and nanochemistry*. Springer; 2006. p. 230.
43. Koch CC, Ovid'ko I, Seal S, Veprek S. *Structural nanocrystalline materials: fundamentals and applications*. Cambridge University Press; 2007. p. 135.
44. Zhang XH, Hilmas GE, Fahrenholtz WG. Synthesis, densification, and mechanical properties of TaB_2. *Mater Lett* 2008;**62**:4251–3.